

Effective-momenta approach for the four-body Coulomb problem

S. D. López,^{1,*} S. Otranto,² and C. R. Garibotti¹

¹CONICET and Centro Atómico Bariloche, Av. Bustillo Km 9.4, 8400 S. C. de Bariloche, Argentina

²IFISUR and Departamento de Física, Universidad Nacional del Sur, 8000 Bahía Blanca, Argentina

(Received 23 November 2012; published 15 February 2013)

We propose approximate separable solutions for the Schrödinger equation corresponding to the four-body Coulomb problem. By exploring several asymptotic limits, we find configurations where the nondiagonal terms of the Hamiltonian can be introduced in the two-body Coulomb-like distortion factors leading to modified momenta. The present effective momenta model is used to study the double ionization of He by ion impact at the fully differential level. Possible differences arising from proton and antiproton impact are explored at impact energies in the range 700 keV/amu–6 MeV/amu. The results are represented in terms of contour plots as a function of the electrons' emission angles, and the four-body dynamics for the double-ionization process is analyzed. Finally, we compare diverse representations for the fully differential cross section. A detailed interpretation of the features of the process is done by overlapping the recoil level lines over the contour plots. Ternary plots are tested as an alternative tool to explore the different physical mechanisms involved in the double emission process at the fully differential level.

DOI: [10.1103/PhysRevA.87.022705](https://doi.org/10.1103/PhysRevA.87.022705)

PACS number(s): 34.10.+x, 34.50.Fa

I. INTRODUCTION

Almost 50 years ago, Vainstein *et al.* introduced the usually denominated Vainshtein Presnyakov and Sobelmann (VPS) method, which represents one of the first proposals to decouple the relative motion of the different pair of particles conforming a three-body Coulomb system [1]. This approximation, in the ion-atom collisions context, assumes that the emitted electron can be described by a Coulomb wave function and leads to a wave equation for the electron-projectile pair. The latter includes a nonseparable Hamiltonian term which was initially neglected in those days. Some years later, Felden and collaborators [2–4], studied the nonseparable terms within the framework of the VPS method. They approximately accounted for the residual Hamiltonian by modifying, at the three-body wave-function level, the impact energy by adding a state-dependent constant. When used to describe the $e + \text{H}(1s) \rightarrow e + \text{H}(2s)$ process, this model led to improved results compared to the Born approximation. The introduction of the 3C wave function [5–8] meant a significant theoretical breakthrough and was widely used in subsequent years to study the ionization of atoms by electron, ion, and photon impact. This approximate analytical model for the three-body continuum consists in the product of three independent Coulomb wave functions corresponding to the three pairs of particles involved. This function satisfies the denominated Redmond asymptotic conditions [9] in the Ω_0 asymptotic region, where the three particles are far apart from each other, and founded the base of many distorted-wave theories [10,11]. During the 1990s several authors worked upon the improvement of the 3C model by considering additional regions (Ω_j , $j = 1, 2, 3$) in which one of the particles is located far away from the remaining pair [12–15] or the Wannier region in which two electrons leave the parent nucleus in a collinear direction [16]. Most of these works make use of dynamical (momentum or coordinate-dependent) effective charges to

account for the correlation terms neglected in the 3C model. Although based on the satisfaction of desirable physical limits, none of these proposals provide a clear indication on how the nondiagonal kinetic-energy terms are explicitly approximated.

These models were soon applied to the evaluation of a triply differential cross section for the ionization of hydrogen by electron impact at fixed momentum transfers [16,17] and photo-double-ionization of He [18] with partial success. The theory of coordinate-dependent momenta was employed by Jones and Madison in the $(e, 2e)$ context obtaining similar results to those presented by Berakdar and Briggs [16] using the 3C and DS3C at intermediate and high electron ejection energies. Nevertheless, these models hardly improved the poor results provided by the 3C at low ejection energies.

Multivariable hypergeometric functions allow an approximate treatment of the nondiagonal kinetic-energy terms [19,20]. These functions couple the two-body motions, satisfy the Kato cusp conditions at the coalescence points, and fulfill the appropriate asymptotic conditions. However, they are not suited for the reaction region where all the particles are close.

Distorted-wave models for four-body systems were studied by Belkic *et al.* [21] but only restricted to the cases in which two or three particles in the final state form a closed separate bounded subsystem. Their distorted-wave models were applied to study transfer-ionization [21] and double-capture processes [22] for He^{2+} collisions on He. An extensive review on four-body distorted-wave models has been published by Belkic *et al.* [23].

By the mid-1990s, Berakdar explored the full four-body continuum problem proposing a product of six Coulomb distortion factors [24]. In recent years, this model was applied in the $(e, 3e)$ context by Götz *et al.* [25], including an extension of the dynamical screening model for a three-electron system.

On the other hand, by the late 1980s, with the rise of new powerful computing systems, full-numerical treatments became feasible and allowed for a more accurate description of atomic processes. In the ion-atom context, the works of Reading and Ford, Díaz *et al.*, and Pindzola *et al.* [26–28] focused on the calculation of total cross sections for double ionization

*sebastian.lopez@cab.cnea.gov.ar

of He as well as the double- to single-ionization ratio values at high impact energies. Their results were in excellent agreement with the available experimental data. For differential cross sections, Foster [29] and Guan [30] calculated in recent years angular distributions for the double ionization of He with the time-dependent close-coupling method, obtaining some discrepancies among each other which must yet be solved.

Nevertheless, for many applications, perturbative approaches based on analytical wave functions are desirable since they provide fast access to the physical mechanisms involved in a collision reaction [31,32] and large accurate-enough data sets can be provided in short periods of time. In this sense, and despite the great numerical advance achieved in the past two decades, the search for an accurate analytical model for the many-body continuum remains an actual challenge and a problem of potential interest.

In this work, we focus on the four-body Coulomb problem in the continuum and propose separable wave functions for the different asymptotic regions which approximately include the information contained in the nonorthogonal kinetic-energy terms. As particular cases of interest, we consider (i) the asymptotic limit where two particles are near each other while the others are far from any of the other three particles and (ii) the limit in which they are arranged as two pairs of particles which are far from each other. In the former, the nondiagonal kinetic terms present in the Schrödinger equation are incorporated in the electron-electron distorted wave via an effective interelectronic momentum. Similarly, in the latter, the present analysis leads to a distorted wave for the interaction among heavy particles, which includes an effective internuclear momentum. In both cases, these effective momenta explicitly depend on the projectile charge. In Sec. III, we use a model based on these effective momenta to evaluate the fully differential cross sections (FDCS) for the double ionization of helium by ion impact within the first Born approximation [33]. In Sec. IV, we compare alternative representations which have been used during the past decade to analyze these FDCS: contour plots and recoil maps. Two-dimensional ternary plots are proposed as a potential tool to highlight the physical mechanisms involved [34,35]. Finally, in Sec. V we draw our conclusions and outlook. Atomic units are used throughout this work unless explicitly stated.

II. THEORETICAL MODEL

We consider a system composed by a projectile and a two active electron atom. The orthogonal Jacobi coordinate system $\{\mathbf{x}_1, \mathbf{X}_1, \sigma\}$ chosen for the four particles in this work is shown in Fig. 1(a) where m_P is the projectile mass, m_T the target

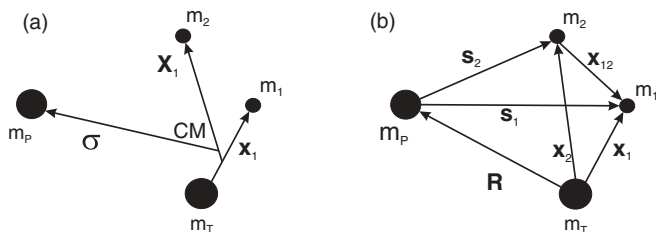


FIG. 1. Coordinate scheme for the four-body problem: (a) Jacobi generalized coordinates and (b) relative coordinates.

core mass, and m_i with $i = 1, 2$ the corresponding electrons masses (which are equal to unity). Here, \mathbf{x}_1 is the position of the first electron relative to the target nucleus, \mathbf{X}_1 represents the relative position of the second electron relative to the center of mass of the nucleus-first electron subsystem, and σ is the relative position of the projectile to the atomic center of mass. When the target nucleus is considered as infinitely massive compared to the electrons, the Jacobi coordinates \mathbf{X}_1 and σ are approximately equal to \mathbf{x}_2 and \mathbf{R} . This situation is illustrated Fig. 1(b) together with the other relative coordinates between the different pairs of particles. Here $\mathbf{s}_i = \mathbf{x}_i - \mathbf{R}$ are the electron-projectile relative positions and $\mathbf{x}_{12} = \mathbf{x}_1 - \mathbf{x}_2$ is the interelectronic position vector. Assuming that the atomic center of mass is located in the atomic core, the four-body Schrödinger equation for this system can be written as

$$\left(-\frac{1}{2\mu_T} \nabla_{\mathbf{x}_1}^2 - \frac{1}{2\mu_T} \nabla_{\mathbf{x}_2}^2 + V_{T_1} + V_{T_2} + V_{12} - \frac{1}{2\nu} \nabla_{\mathbf{R}}^2 + V_{P_1} + V_{P_2} + V_{PT} \right) \Psi_f = E \Psi_f. \quad (1)$$

The quantity $\mu_T = \frac{m_T}{m_T+1}$ is the reduced mass of each electron relative to the atomic core, while $\mu_P = \frac{m_P}{m_P+1}$ is the reduced mass of each electron relative to the projectile. The reduced mass between the projectile and the target core is $\nu = \frac{m_P m_T}{m_P + m_T}$. The potential term $V_{T_i} = Z_T Z_i / x_i$, is the Coulomb interaction of electron i with the target core, $V_{12} = 1/x_{12}$ is the interelectronic repulsion, $V_{PT} = Z_P Z_T / R$ is the projectile-atomic core interaction, and $V_{P_i} = Z_P Z_i / s_i$ represents the Coulomb interaction between electron i and the projectile.

On the other hand, the conjugate momenta associated to the Jacobi coordinates here used are $\{\mathbf{k}_1, \mathbf{K}_1, \mathbf{K}_\sigma\}$. Here, \mathbf{k}_1 is the momentum of one electron relative to the target, \mathbf{K}_1 is the momentum of the second electron relative to the electron-nucleus subsystem, and \mathbf{K}_σ denotes the momentum of the projectile relative to the whole atom. It is important to note that for an infinitely massive target nucleus $\mathbf{K}_1 \approx \mathbf{k}_2$ and $\mathbf{K}_\sigma \approx \mathbf{K}_f$. The total energy for the four-body continuum is then given by

$$E = \frac{K_f^2}{2\nu} + \frac{k_1^2}{2\mu_T} + \frac{k_2^2}{2\mu_T}. \quad (2)$$

For further developments it is convenient to define the remaining relative momenta of the four particles as follows: $\mathbf{k}_{12} = (\mathbf{k}_1 - \mathbf{k}_2)/2$ the relative momentum between the electrons and $\mathbf{p}_i = \mathbf{k}_i(\mu_P/\mu_T) - \mathbf{K}_f(\mu_P/\nu)$ the momentum of the i th electron relative to the projectile.

Since we are concerned with continuum states, we propose the following solution for the four-body system in the continuum:

$$\begin{aligned} \Psi_f &= e^{i\mathbf{K}_f \cdot \mathbf{R}} e^{i\mathbf{k}_1 \cdot \mathbf{x}_1} e^{i\mathbf{k}_2 \cdot \mathbf{x}_2} \varphi_{\mathbf{k}_1}(\mathbf{x}_1) \varphi_{\mathbf{k}_2}(\mathbf{x}_2) \varphi_{\mathbf{k}_{12}}(\mathbf{x}_{12}) \\ &\quad \times \varphi_{\mathbf{p}_1}(\mathbf{s}_1) \varphi_{\mathbf{p}_2}(\mathbf{s}_2) \varphi_{\mathbf{K}_f}(\mathbf{R}) \\ &= e^{i\mathbf{K}_f \cdot \mathbf{R}} e^{i\mathbf{k}_1 \cdot \mathbf{x}_1} e^{i\mathbf{k}_2 \cdot \mathbf{x}_2} \chi_f(\mathbf{x}_1, \mathbf{x}_2, \mathbf{R}). \end{aligned} \quad (3)$$

This functional form accounts for the removal of the kinetic-energy terms off the Schrödinger equation via the plane-wave factors. In addition, the separable nature of the distorted waves proposed in the different relative coordinates provide a conve-

nient route to analytically explore the distortion effects induced by the Coulomb potentials $V_{T_1}, V_{T_2}, V_{12}, V_{P_1}, V_{P_2}$, and V_{PT} .

Inserting this function into Eq. (1), we obtain

$$(H - E)\chi_f = \left(-\frac{1}{2\mu_T} \nabla_{x_1}^2 - \frac{i}{\mu_T} \mathbf{k}_1 \cdot \nabla_{x_1} - \frac{1}{2\mu_T} \nabla_{x_2}^2 - \frac{i}{\mu_T} \mathbf{k}_2 \cdot \nabla_{x_2} + V_{T_1} + V_{T_2} + V_{12} - \frac{1}{2\nu} \nabla_R^2 - \frac{i}{\nu} \mathbf{K}_f \cdot \nabla_{\mathbf{R}} + V_{P_1} + V_{P_2} + V_{PT} \right) \chi_f. \quad (4)$$

To evaluate how the differential operators act on the χ_f function, we note that $\nabla_{x_i} \varphi_{p_i}(\mathbf{s}_i) = \nabla_{s_i} \varphi_{p_i}(\mathbf{s}_i)$, $\nabla_{\mathbf{R}} \varphi_{p_i}(\mathbf{s}_i) = -\nabla_{s_i} \varphi_{p_i}(\mathbf{s}_i)$, $\nabla_{x_1} \varphi_{k_{12}}(\mathbf{x}_{12}) = \nabla_{x_{12}} \varphi_{k_{12}}(\mathbf{x}_{12})$, and $\nabla_{x_2} \varphi_{k_{12}}(\mathbf{x}_{12}) = -\nabla_{x_{12}} \varphi_{k_{12}}(\mathbf{x}_{12})$. Introducing these expressions into Eq. (4), and after a lengthy algebra, we find

$$(H - E)\chi_f = \left[\sum_{j=1,2} \left(-\frac{1}{2\mu_T} \frac{\nabla_{x_j}^2 \varphi_{k_j}(\mathbf{x}_j)}{\varphi_{k_j}(\mathbf{x}_j)} - \frac{i}{\mu_T} \mathbf{k}_j \cdot \mathbf{G}_{k_j}(\mathbf{x}_j) + V_{T_j} \right) + \left(-\frac{1}{2\mu_{12}} \frac{\nabla_{x_{12}}^2 \varphi_{k_{12}}(\mathbf{x}_{12})}{\varphi_{k_{12}}(\mathbf{x}_{12})} - \frac{i}{\mu_{12}} \mathbf{k}_{12} \cdot \mathbf{G}_{k_{12}}(\mathbf{x}_{12}) + V_{12} \right) + \sum_{j=1,2} \left(-\frac{1}{2\mu_P} \frac{\nabla_{s_j}^2 \varphi_{p_j}(\mathbf{s}_j)}{\varphi_{p_j}(\mathbf{s}_j)} - \frac{i}{\mu_P} \mathbf{p}_j \cdot \mathbf{G}_{p_j}(\mathbf{s}_j) + V_{P_j} \right) + \left(-\frac{1}{2\nu} \frac{\nabla_R^2 \varphi_{K_f}(\mathbf{R})}{\varphi_{K_f}(\mathbf{R})} - \frac{i}{\nu} \mathbf{K}_f \cdot \mathbf{G}_{K_f}(\mathbf{R}) + V_{PT} \right) + H_{ND} \right] \chi_f, \quad (5)$$

where

$$\mathbf{G}_{\mathbf{k}}(\mathbf{r}) = \frac{\nabla_{\mathbf{r}} \varphi_{\mathbf{k}}(\mathbf{r})}{\varphi_{\mathbf{k}}(\mathbf{r})} \quad (6)$$

is a functional operator acting on the φ function. Here \mathbf{r} and \mathbf{k} are used to indicate any of the involved coordinates and momenta.

In Eq. (5), H_{ND} represents the nondiagonal terms of the Hamiltonian which for the present coordinate system are given by

$$H_{ND}\chi_f = \left(\frac{1}{\mu_T} [\mathbf{G}_{k_2}(\mathbf{x}_2) - \mathbf{G}_{k_1}(\mathbf{x}_1) - \mathbf{G}_{p_1}(\mathbf{s}_1) + \mathbf{G}_{p_2}(\mathbf{s}_2)] \cdot \mathbf{G}_{k_{12}}(\mathbf{x}_{12}) - \frac{1}{\mu_T} \mathbf{G}_{p_1}(\mathbf{s}_1) \cdot \mathbf{G}_{k_1}(\mathbf{x}_1) - \frac{1}{\mu_T} \mathbf{G}_{p_2}(\mathbf{s}_2) \cdot \mathbf{G}_{k_2}(\mathbf{x}_2) + \frac{1}{\nu} \mathbf{G}_{K_f}(\mathbf{R}) \cdot [\mathbf{G}_{p_2}(\mathbf{s}_2) + \mathbf{G}_{p_1}(\mathbf{s}_1)] - \frac{1}{\nu} \mathbf{G}_{p_1}(\mathbf{s}_1) \cdot \mathbf{G}_{p_2}(\mathbf{s}_2) \right) \chi_f. \quad (7)$$

When H_{ND} is neglected, an exact separable solution is found for Eq. (5). In this case, the wave function χ_f becomes a 12C function:

$$\chi_f(\mathbf{x}_1, \mathbf{x}_2, \mathbf{R}) = \chi_f^+(\mathbf{x}_1, \mathbf{x}_2, \mathbf{R}) \chi_f^-(\mathbf{x}_1, \mathbf{x}_2, \mathbf{R}), \quad (8)$$

$$\chi_f^\pm(\mathbf{x}_1, \mathbf{x}_2, \mathbf{R}) = D_{k_1}^\pm(\mathbf{x}_1) D_{k_2}^\pm(\mathbf{x}_2) D_{k_{12}}^\pm(\mathbf{x}_{12}) D_{p_1}^\pm(\mathbf{s}_1) \times D_{p_2}^\pm(\mathbf{s}_2) D_{K_f}^\pm(\mathbf{R}), \quad (9)$$

where the minus and plus signs are associated to outgoing or incoming boundary conditions, respectively. This wave function is the four-body problem generalization of the 6C wave function found for the three-body problem [19]. When incoming boundary conditions are considered for the wave function, the proposed solution reduces to a product of six Kummer hypergeometric functions (3C in the three-body problem [5,7]).

A step forward in the present analysis is made by proposing known functional forms for some of the functions in Eq. (3). By so doing, we are led to a new set of coupled equations for the unknown remaining functions in Eq. (5).

Clearly, the adequate choice for a function that describes the two-body Coulomb distortion is the well-known Kummer hypergeometric function:

$$D_{\mathbf{k}}^\pm(\mathbf{r}) = N^\pm(k) {}_1F_1[\mp i\eta, 1, \pm i(kr \mp \mathbf{k} \cdot \mathbf{r})], \quad (10)$$

which is a solution of

$$\left(-\frac{1}{2\mu} \nabla^2 + \frac{Z}{r} \right) D_{\mathbf{k}}^\pm(\mathbf{r}) = i \frac{\mathbf{k}}{\mu} \cdot \nabla D_{\mathbf{k}}^\pm(\mathbf{r}). \quad (11)$$

As an example, if five Coulomb distortion factors are proposed in Eq. (3), the only function left undetermined is φ_{K_f} , which depends on \mathbf{R}, \mathbf{x}_1 and \mathbf{x}_2 . As expected, the corresponding differential equation concentrates the information on the whole four-body coupling. Unfortunately, analytical solutions for this remaining equation are unknown and further approximations are required in order to gain insight into the problem. In the next sections we analyze physically meaningful asymptotic limits and propose analytical wave functions which go beyond the simple 12C function.

A. Asymptotic regions

In the following, we summarize several asymptotic limits for the four-body system in the continuum. Based on the fact that a closed analytical solution for the three-body problem is not available yet, in this work we consider neither the condensation region (where all the particles are close) nor the situation in which three of the particles are close while the remaining one is far from this subsystem. Instead, we generate analytical models which go beyond the simple 6C model by satisfying the proper asymptotic conditions in the denominated Υ , Γ , and Λ regions, which are defined as follows.

(i) Υ . The four particles are far away from each other: $x_{1,2} \rightarrow \infty$, $s_{1,2} \rightarrow \infty$, $x_{12} \rightarrow \infty$, and $R \rightarrow \infty$. In this region, all the two-body solutions are asymptotically correct, and they can be replaced by eikonal functions. The terms conforming $H_{\text{ND}}\chi_f$ are of order $O(1/r^2)$, and can be neglected.

(ii) Γ_1 . The electrons are close together: $x_{1,2} \rightarrow \infty$, $s_{1,2} \rightarrow \infty$, $R \rightarrow \infty$, $x_{12}/x_{1,2} \rightarrow 0$, $x_{12}/s_{1,2} \rightarrow 0$, and $x_{12}/R \rightarrow 0$.

(iii) Γ_2 . One electron is close to the projectile: $s_i \rightarrow \infty$, $x_{1,2} \rightarrow \infty$, $x_{12} \rightarrow \infty$, $R \rightarrow \infty$, $s_j/s_i \rightarrow 0$, $s_j/x_{1,2} \rightarrow 0$, $s_j/x_{12} \rightarrow 0$, and $s_j/R \rightarrow 0$.

(iv) Γ_3 . One electron is close to the target nucleus: $x_i \rightarrow \infty$, $s_{1,2} \rightarrow \infty$, $x_{12} \rightarrow \infty$, $R \rightarrow \infty$, $x_j/x_i \rightarrow 0$, $x_j/x_{12} \rightarrow 0$, $x_j/s_{1,2} \rightarrow 0$, and $x_j/R \rightarrow 0$.

(v) Γ_4 . The projectile is close to the target nucleus: $x_{1,2} \rightarrow \infty$, $x_{12} \rightarrow \infty$, $s_{1,2} \rightarrow \infty$, $R/x_{1,2} \rightarrow 0$, $R/s_{1,2} \rightarrow 0$, and $R/x_{12} \rightarrow 0$.

(vi) Λ_1 . One electron is close to the target nucleus and the other is close to the projectile: $x_i \rightarrow \infty$, $x_{12} \rightarrow \infty$, $s_j \rightarrow \infty$, $R \rightarrow \infty$, $x_j/x_i \rightarrow 0$, $x_j/x_{12} \rightarrow 0$, $x_j/s_j \rightarrow 0$, $x_j/R \rightarrow 0$, $s_i/x_i \rightarrow 0$, $s_i/x_{12} \rightarrow 0$, $s_i/s_j \rightarrow 0$, and $s_i/R \rightarrow 0$.

(vii) Λ_2 . One electron is close to the other and the heavy particles are close together: $x_{1,2} \rightarrow \infty$, $s_{1,2} \rightarrow \infty$, $x_{12}/x_{1,2} \rightarrow 0$, $x_{12}/s_{1,2} \rightarrow 0$, $R/x_{1,2} \rightarrow 0$, and $R/s_{1,2} \rightarrow 0$.

For the Γ_1 region the wave function can then be written as (incoming boundary conditions will be used in what follows)

$$\chi_f(\mathbf{x}_1, \mathbf{x}_2, \mathbf{R}) = D_{\mathbf{k}_1}(\mathbf{x}_1)D_{\mathbf{k}_2}(\mathbf{x}_2)\varphi_{\mathbf{k}_{12}}(\mathbf{x}_{12})D_{\mathbf{p}_1}(\mathbf{s}_1) \times D_{\mathbf{p}_2}(\mathbf{s}_2)D_{\mathbf{K}_f}(\mathbf{R}). \quad (12)$$

Neglecting terms $O(1/r^2)$ in the asymptotic variables, the $\varphi_{\mathbf{k}_{12}}(\mathbf{x}_{12})$ function must be a solution of

$$(H - E)\chi_f = \left[-\frac{1}{2\mu_{12}} \frac{\nabla_{\mathbf{x}_{12}}^2 \varphi_{\mathbf{k}_{12}}(\mathbf{x}_{12})}{\varphi_{\mathbf{k}_{12}}(\mathbf{x}_{12})} - \left(i \frac{\mathbf{k}_{12}}{\mu_{12}} - \frac{1}{\mu_T} \mathbf{F}_{\mathbf{k}_2}(\mathbf{x}_2) + \frac{1}{\mu_T} \mathbf{F}_{\mathbf{k}_1}(\mathbf{x}_1) + \frac{1}{\mu_T} \mathbf{F}_{\mathbf{p}_1}(\mathbf{s}_1) - \frac{1}{\mu_T} \mathbf{F}_{\mathbf{p}_2}(\mathbf{s}_2) \right) \cdot \nabla_{\mathbf{x}_{12}} \varphi_{\mathbf{k}_{12}}(\mathbf{x}_{12}) + V_{12} \right] \chi_f, \quad (13)$$

where we have made use of the functional operator introduced by Berakdar [13]:

$$\mathbf{F}_{\mathbf{k}}(\mathbf{r}) = \frac{\nabla_{\mathbf{r}} D_{\mathbf{k}}(\mathbf{r})}{D_{\mathbf{k}}(\mathbf{r})}. \quad (14)$$

Provided that the asymptotic limit of this operator has a closed analytical form,

$$\mathbf{F}_{\mathbf{k}}(\mathbf{r}) \rightarrow \mathbf{E}_{\mathbf{k}}(\mathbf{r}) = \frac{i\mu Z (\hat{\mathbf{k}} + \hat{\mathbf{r}})}{kr(1 + \hat{\mathbf{k}} \cdot \hat{\mathbf{r}})}, \quad (15)$$

for $r \rightarrow \infty$, and the Schrödinger equation in the Γ_1 region is given by

$$(H - E)\chi_f = \frac{1}{\varphi_{\mathbf{k}_{12}}(\mathbf{x}_{12})} \left[-\frac{1}{2\mu_{12}} \nabla_{\mathbf{x}_{12}}^2 \varphi_{\mathbf{k}_{12}}(\mathbf{x}_{12}) - i \left(\frac{\mathbf{k}_{12}}{\mu_{12}} - \frac{1}{\mu_T} \mathbf{E}_{\mathbf{k}_2}(\mathbf{x}_2) + \frac{1}{\mu_T} \mathbf{E}_{\mathbf{k}_1}(\mathbf{x}_1) - \frac{1}{\mu_T} \mathbf{E}_{\mathbf{p}_1}(\mathbf{s}_1) + \frac{1}{\mu_T} \mathbf{E}_{\mathbf{p}_2}(\mathbf{s}_2) \right) \cdot \nabla_{\mathbf{x}_{12}} \varphi_{\mathbf{k}_{12}}(\mathbf{x}_{12}) + V_{12} \varphi_{\mathbf{k}_{12}}(\mathbf{x}_{12}) \right] \chi_f. \quad (16)$$

The $\varphi_{\mathbf{k}_{12}}(\mathbf{x}_{12})$ function describes the relative motion of the two close particles, and must be a solution of a differential equation similar to the Coulomb equation, with an additional first-order derivative term which couples the equation to the other variables. In the next section we propose different alternative approximations to deal with this term.

A similar procedure for the Γ_3 region leads to

$$\chi_f(\mathbf{x}_1, \mathbf{x}_2, \mathbf{R}) = \varphi_{\mathbf{k}_1}(\mathbf{x}_1)D_{\mathbf{k}_2}(\mathbf{x}_2)D_{\mathbf{k}_{12}}(\mathbf{x}_{12})D_{\mathbf{p}_1}(\mathbf{s}_1)D_{\mathbf{p}_2}(\mathbf{s}_2)D_{\mathbf{K}_f}(\mathbf{R}). \quad (17)$$

In this particular case, the resulting asymptotic equation for $\varphi_{\mathbf{k}_1}(\mathbf{x}_1)$ reads

$$(H - E)\chi_f = \frac{1}{\varphi_{\mathbf{k}_1}(\mathbf{x}_1)} \left[-\frac{1}{2\mu_T} \nabla_{\mathbf{x}_1}^2 \varphi_{\mathbf{k}_1}(\mathbf{x}_1) - i \left(\frac{\mathbf{k}_1}{\mu_T} + \frac{1}{\mu_T} \mathbf{E}_{\mathbf{k}_{12}}(\mathbf{x}_{12}) - \frac{1}{\mu_T} \mathbf{E}_{\mathbf{p}_1}(\mathbf{s}_1) \right) \cdot \nabla_{\mathbf{x}_1} \varphi_{\mathbf{k}_1}(\mathbf{x}_1) + V_{T1} \varphi_{\mathbf{k}_1}(\mathbf{x}_1) \right] \chi_f. \quad (18)$$

For the other Γ regions similar equations can be derived applying the same method.

In the Λ_1 region we write

$$\chi_f(\mathbf{x}_1, \mathbf{x}_2, \mathbf{R}) = \varphi_{\mathbf{k}_1}(\mathbf{x}_1)D_{\mathbf{k}_2}(\mathbf{x}_2)D_{\mathbf{k}_{12}}(\mathbf{x}_{12})D_{\mathbf{p}_1}(\mathbf{s}_1)\varphi_{\mathbf{p}_2}(\mathbf{s}_2)D_{\mathbf{K}_f}(\mathbf{R}). \quad (19)$$

The asymptotic equation for $\varphi_{\mathbf{k}_1}(\mathbf{x}_1)$ and $\varphi_{\mathbf{p}_2}(\mathbf{s}_2)$ reads in this case

$$(H - E)\chi_f = \left\{ \frac{1}{\varphi_{\mathbf{k}_1}(\mathbf{x}_1)} \left(-\frac{1}{2\mu_T} \nabla_{\mathbf{x}_1}^2 \varphi_{\mathbf{k}_1}(\mathbf{x}_1) - \frac{i}{\mu_T} [\mathbf{k}_1 + \mathbf{E}_{\mathbf{k}_{12}}(\mathbf{x}_{12}) - \mathbf{E}_{\mathbf{p}_1}(\mathbf{s}_1)] \cdot \nabla_{\mathbf{x}_1} \varphi_{\mathbf{k}_1}(\mathbf{x}_1) + V_{T1} \varphi_{\mathbf{k}_1}(\mathbf{x}_1) \right) + \frac{1}{\varphi_{\mathbf{p}_2}(\mathbf{s}_2)} \left[-\frac{1}{2\mu_P} \nabla_{\mathbf{s}_2}^2 \varphi_{\mathbf{p}_2}(\mathbf{s}_2) - \frac{i}{\mu_P} \left(\mathbf{p}_2 - \frac{\mu_P}{\mu_T} \mathbf{E}_{\mathbf{k}_{12}}(\mathbf{x}_{12}) - \frac{\mu_P}{\mu_T} \mathbf{E}_{\mathbf{k}_2}(\mathbf{x}_2) - \frac{\mu_P}{\nu} \mathbf{E}_{\mathbf{K}_f}(\mathbf{R}) - \frac{\mu_P}{\nu} \mathbf{E}_{\mathbf{p}_1}(\mathbf{s}_1) \right) \cdot \nabla_{\mathbf{s}_2} \varphi_{\mathbf{p}_2}(\mathbf{s}_2) + V_{P2} \varphi_{\mathbf{p}_2}(\mathbf{s}_2) \right] \right\} \chi_f. \quad (20)$$

As the last particular case here studied, we consider the Λ_2 region for which we propose

$$\chi_f(\mathbf{x}_1, \mathbf{x}_2, \mathbf{R}) = D_{\mathbf{k}_1}(\mathbf{x}_1)D_{\mathbf{k}_2}(\mathbf{x}_2)\varphi_{\mathbf{k}_{12}}(\mathbf{x}_{12})D_{\mathbf{p}_1}(\mathbf{s}_1)D_{\mathbf{p}_2}(\mathbf{s}_2)\varphi_{\mathbf{K}_f}(\mathbf{R}). \quad (21)$$

The asymptotic Schrödinger equation in the Λ_2 region is then given by

$$(H - E)\chi_f = \left\{ \frac{1}{\varphi_{\mathbf{k}_{12}}(\mathbf{x}_{12})} \left[-\frac{1}{2\mu_{12}} \nabla_{\mathbf{x}_{12}}^2 \varphi_{\mathbf{k}_{12}}(\mathbf{x}_{12}) - \frac{i}{\mu_T} \left(\frac{\mu_T}{\mu_{12}} \mathbf{k}_{12} + \mathbf{E}_{\mathbf{k}_2}(\mathbf{x}_2) - \mathbf{E}_{\mathbf{k}_1}(\mathbf{x}_1) - \mathbf{E}_{\mathbf{p}_1}(\mathbf{s}_1) + \mathbf{E}_{\mathbf{p}_2}(\mathbf{s}_2) \right) \cdot \nabla_{\mathbf{x}_{12}} \varphi_{\mathbf{k}_{12}}(\mathbf{x}_{12}) + V_{12} \varphi_{\mathbf{k}_{12}}(\mathbf{x}_{12}) \right] + \frac{1}{\varphi_{\mathbf{K}_f}(\mathbf{R})} \left(-\frac{1}{2\nu} \nabla_{\mathbf{R}}^2 \varphi_{\mathbf{K}_f}(\mathbf{R}) - \frac{i}{\nu} [\mathbf{K}_f - \mathbf{E}_{\mathbf{p}_2}(\mathbf{s}_2) + \mathbf{E}_{\mathbf{p}_1}(\mathbf{s}_1)] \cdot \nabla_{\mathbf{R}} \varphi_{\mathbf{K}_f}(\mathbf{R}) + V_{PT} \varphi_{\mathbf{K}_f}(\mathbf{R}) \right) \right\} \chi_f. \quad (22)$$

We note that Eqs. (13), (16), (18), (20), and (22) all consist in sums of differential equations which resemble the two-body Coulomb problem. However, we note that the factors multiplying the terms involving gradients do not consist of the typical momenta but instead can be interpreted as coordinate-dependent effective momenta. These effective momenta are the sum of the corresponding two-body asymptotic momentum plus coordinate-dependent vectors that account for the nondiagonal Hamiltonian contribution [Eq. (7)]. In other words, at the asymptotic regions under study, the information contained in the nondiagonal terms can be associated to a particular two-body subsystem. These effective momenta account for the four-body correlations at nonasymptotic distances, since the momenta depend on the four-body coordinates. As all the interparticle distances tend to infinite, the H_{ND} terms incorporated by these effective momenta vanish and the 6C model is naturally recovered.

In early works developed for the three-body problem [12,14,15], the common assumption was that the linear correction terms were independent (or slowly varying functions) of the coordinates in the differential equation, leading to a coordinate-dependent effective momenta. However, such an assumption implies to neglect all the derivatives in terms of coordinates of the correction terms in the corresponding differential equation. Since the effective momenta derivative is $O(1/r)$, the Sommerfeld parameter $a(\mathbf{r})$ is proportional to r and their derivative scale is of zeroth order in r . This becomes clear by looking at the series expression for the hypergeometric function:

$${}_1F_1\{a(\mathbf{r}), 1, i[k(\mathbf{r})r + \mathbf{k}(\mathbf{r}) \cdot \mathbf{r}]\} = \sum_n \frac{[a(\mathbf{r})]_n}{n!} i^n [k(\mathbf{r})r + \mathbf{k}(\mathbf{r}) \cdot \mathbf{r}]^n. \quad (23)$$

A complete treatment of the derivatives in the parameters of the hypergeometric functions can be found in a recent paper by Ancarani and Gasaneo [36]. At this point, further approximations need to be made to retain the functional form of the Kummer hypergeometric function.

B. Approximations in the momentum formalism

Depending on the process under consideration, only some terms of the nondiagonal kinetic energy will prevail, determining the relevance of the different asymptotic regions. Now we will consider the Γ_1 region, where the relevance of the $e-e$ correlation is enhanced for atomic double-ionization collisions which are mediated by the denominated two-step-1 (TS1)

mechanism in which the projectile hits an electron first, which in a subsequent stage hits and removes a second one.

The easiest assumption is to consider coordinate-independent nondiagonal kinetic energy terms, by taking fixed physically meaningful interparticle distances and directions. For atomic double ionization by bare ion impact, the following approximations are made.

(a) First, we consider the asymptotic emission geometry: $\hat{\mathbf{x}}_i \parallel \hat{\mathbf{k}}_i$ and $\hat{\mathbf{s}}_i \parallel \hat{\mathbf{p}}_i$ [37].

(b) The reaction zone around the target is limited by the Wannier radius (R_W). Outside this radius the electrons-target ion motion is well described by an eikonal wave. We use Rau's expression for the Wannier radius [38],

$$R_{WT} = 4\sqrt{2}(Z_T - 1/4)/(k_1^2 + k_2^2). \quad (24)$$

(c) To obtain a reference value for the projectile-electron distances, we define the characteristic time $\tau_i = R_{WT}/k_i$ and approximate the projectile-electron distance by

$$R_{CS_i} = |\tau_i \mathbf{v}_P + \mathbf{b} - R_{WT} \hat{\mathbf{k}}_i|. \quad (25)$$

The impact parameter b value is such that the reduced probability function $bP(b)$ for single ionization has its maximum. These probabilities are calculated with the continuum distorted-wave-eikonal initial state method, for each collision energy. As a result, each electron sees an effective relative distance with respect to the projectile which is associated to its emission energy and direction.

With these hypotheses the relative electron-electron motion in the Γ_1 region can be described by a Coulomb wave function with a modified momentum given by

$$\tilde{\mathbf{k}}_{12} = \mathbf{k}_{12} + \frac{\mu_{12} Z_T \hat{\mathbf{k}}_1}{k_1 R_W} - \frac{\mu_{12} Z_T \hat{\mathbf{k}}_2}{k_2 R_W} + \frac{\mu_{12} \mu_P Z_P \hat{\mathbf{p}}_1}{\mu_T p_1 R_{CS_1}} - \frac{\mu_{12} \mu_P Z_P \hat{\mathbf{p}}_2}{\mu_T p_2 R_{CS_2}}, \quad (26)$$

Although other similar physical pictures can be used to approximate the nondiagonal terms of the kinetic-energy operator, we find that conditions (a)–(c) provide an instantaneous picture of the system at the time at which each electron reaches the characteristic radius R_{WT} . In Sec. III we use the effective momentum given by Eq. (26) in the evaluation of the FDSC for double ionization of helium by ion impact.

C. Reduction of the four-body solution to the particular three-body case

The present proposal naturally reduces to its three-body limits when the charge and the associated kinetic-energy term

of any of the particles involved are turned off. Two cases will now be considered: (a) two electrons and a heavy particle [($e, 2e$) processes, photo-double-ionization of atoms] and (b) one electron in the field of two heavy centers (atomic single ionization by ion impact).

In first place we consider case (a). In this case, any possible reference to the projectile is removed at the wave-function level. In this case, Eq. (13) is given by

$$(H - E)\chi_f^{3B} = \left\{ \frac{1}{\varphi_{\mathbf{k}_{12}}(\mathbf{x}_{12})} \left[-\frac{1}{2\mu_{12}} \nabla_{\mathbf{x}_{12}}^2 \varphi_{\mathbf{k}_{12}}(\mathbf{x}_{12}) - \left(\frac{i}{\mu_{12}} \mathbf{k}_{12} \right) + \frac{iZ_T(\hat{\mathbf{k}}_2 + \hat{\mathbf{x}}_2)}{k_2 x_2 (1 + \hat{\mathbf{k}}_2 \cdot \hat{\mathbf{x}}_2)} - \frac{iZ_T(\hat{\mathbf{k}}_1 + \hat{\mathbf{x}}_1)}{k_1 x_1 (1 + \hat{\mathbf{k}}_1 \cdot \hat{\mathbf{x}}_1)} \right] \cdot \nabla_{\mathbf{x}_{12}} \varphi_{\mathbf{k}_{12}}(\mathbf{x}_{12}) + V_{12} \varphi_{\mathbf{k}_{12}}(\mathbf{x}_{12}) \right\} \chi_f^{3B}. \quad (27)$$

When the Wannier radius is considered as the characteristic electronic distance, the interelectronic effective momentum results:

$$\tilde{\mathbf{k}}_{12} = \mathbf{k}_{12} + \frac{\mu_{12} Z_T \hat{\mathbf{k}}_1}{k_1 R_{WT}} - \frac{\mu_{12} Z_T \hat{\mathbf{k}}_2}{k_2 R_{WT}}. \quad (28)$$

This effective momentum and the related differential equation can be compared with the one derived by Macri *et al.* [15] in parabolic coordinates for their Ω_3 region [Eq. (23) in their article]. A similar derivation can be made for their $\Omega_{1,2}$ regions.

We now turn our attention to case (b) in which we explore the limit in which all the interactions and coordinates of the second electron in Eq. (21) are removed. For the Λ_2 region, we then obtain

$$\tilde{\mathbf{K}}_f = \mathbf{K}_f + \frac{\mu_P Z_P \hat{\mathbf{p}}_1}{p_1 R_{CS_1}}. \quad (29)$$

From this expression, we note that when the electron is located between the two heavy particles (N- e -N) the internuclear (NN) effective relative momentum \tilde{K}_f decreases compared to K_f . In contrast, when the electron is found along the internuclear axis but on either side (e -N-N or N-N- e), \tilde{K}_f is increased compared to K_f .

III. DOUBLE-IONIZATION CROSS SECTIONS

In this section we test the models previously introduced and with this aim we focus on the double ionization of He by bare ion impact. We explore the range of intermediate to high impact energies, assuming a first-order interaction between the projectile and the target atom. Within this context, the FDCS can be written as

$$\frac{d\sigma}{d\mathbf{k}_1 d\mathbf{k}_2 d\mathbf{Q}_\perp} = \frac{(2\pi)^4}{v_p^2} |T_{fi}|^2. \quad (30)$$

Here, \mathbf{Q}_\perp is the perpendicular component (with respect to the beam axis) of the momentum transferred by the projectile which can be defined as $\mathbf{Q} = \mathbf{K}_i - \mathbf{K}_f$. The first-order transition matrix T_{fi} in a distorted-wave formalism is given by

$$T_{fi} = \langle \chi_f^- | W_i | \chi_i^+ \rangle, \quad (31)$$

where the operator W_i represents the unsolved part of the initial Hamiltonian:

$$W_i = \frac{Z_P Z_T}{R} - \frac{Z_P}{|\mathbf{R} - \mathbf{x}_1|} - \frac{Z_P}{|\mathbf{R} - \mathbf{x}_2|}. \quad (32)$$

The initial state is given by

$$\chi_i^+ = \frac{1}{(2\pi)^{3/2}} e^{i\mathbf{K}_i \cdot \mathbf{R}} \Psi_i^+(\mathbf{x}_1, \mathbf{x}_2). \quad (33)$$

For the atomic ground state we propose [39]

$$\Psi_i^+(\mathbf{x}_1, \mathbf{x}_2) = N_i (e^{-ax_1 - bx_2} + e^{-bx_1 - ax_2}) (e^{-z_c x_{12}} + C_0 e^{-\lambda x_{12}}), \quad (34)$$

with variational parameters $N_i = 1.9358$, $a = 1.4126$, $b = 2.2068$, $\lambda = 0.199$, $C_0 = -0.6649$, and $z_c = 0.01$. This wave function includes initial angular correlation (through the explicit x_{12} dependence) and leads to an energy $\langle E \rangle = -2.9019$ a.u., only 0.0489 eV apart from the exact energy -2.9037 a.u. This wave function differs from the original Bonham and Kohl wave function in the $e^{-z_c x_{12}}$ factor which replaces the 1 appearing in the original function, and provides a convergence factor for integration purposes.

For high impact energies and low Q values the double emission is mediated by the TS1 mechanism. It seems clear for this case that the best possible description of the interelectronic correlation is needed (Γ_1 asymptotic region). Therefore, we propose for the final state

$$\chi_f(\mathbf{x}_1, \mathbf{x}_2, \mathbf{R}) = D_{\mathbf{k}_1}(\mathbf{x}_1) D_{\mathbf{k}_2}(\mathbf{x}_2) \varphi_{\mathbf{k}_{12}}(\mathbf{x}_{12}) D_{\mathbf{p}_1}(\mathbf{s}_1) \times D_{\mathbf{p}_2}(\mathbf{s}_2) D_{\mathbf{K}_f}(\mathbf{R}), \quad (35)$$

where

$$\varphi_{\mathbf{k}_{12}}(\mathbf{x}_{12}) = D_{\tilde{\mathbf{k}}_{12}}(\mathbf{x}_{12}) \quad (36)$$

and $\tilde{\mathbf{k}}_{12}$ is given by Eq. (26). As calculations using the full 6C functions demand a prohibitive amount of time, we replace the hypergeometric functions in the electron-projectile coordinates \mathbf{s}_1 and \mathbf{s}_2 by their corresponding Coulomb factors [8]. The Gramm-Schmidt procedure has been used in all cases in the forthcoming analysis, to account for the orthogonalization of the final to initial atomic state.

In the following, we evaluate the cross sections given by Eq. (30) for proton and antiproton impact on He, at impact energies in the range 700 keV–6 MeV, with a momentum transfer value $Q = 0.9$. We describe the calculated FDCSs for double ionization of He in the coplanar emission geometry (\mathbf{Q} , \mathbf{k}_1 , and \mathbf{k}_2 all laying in the scattering plane defined by \mathbf{K}_i and \mathbf{K}_f), and we represent them in terms of contour plots as a function of the electron emission angles θ_1 and θ_2 with respect to the forward beam axis direction. In Figs. 2(a)–2(c) we show the FDCSs for 700-keV proton impact ($\theta_Q = 40.18^\circ$), when the electrons are ejected with equal energies of 3, 10, and 15 eV, respectively. In Figs. 2(d)–2(f) similar results for antiproton impact are shown.

The first thing we note is that in all cases the FDCS show maxima for electronic emission configurations at which $\mathbf{k}_1 + \mathbf{k}_2$ is either parallel or antiparallel to \mathbf{Q} . We will refer to these maxima as “binary peak” and “recoil peak,” respectively, based on the similarities found with their analog counterparts for single-ionization processes which we now describe [40].

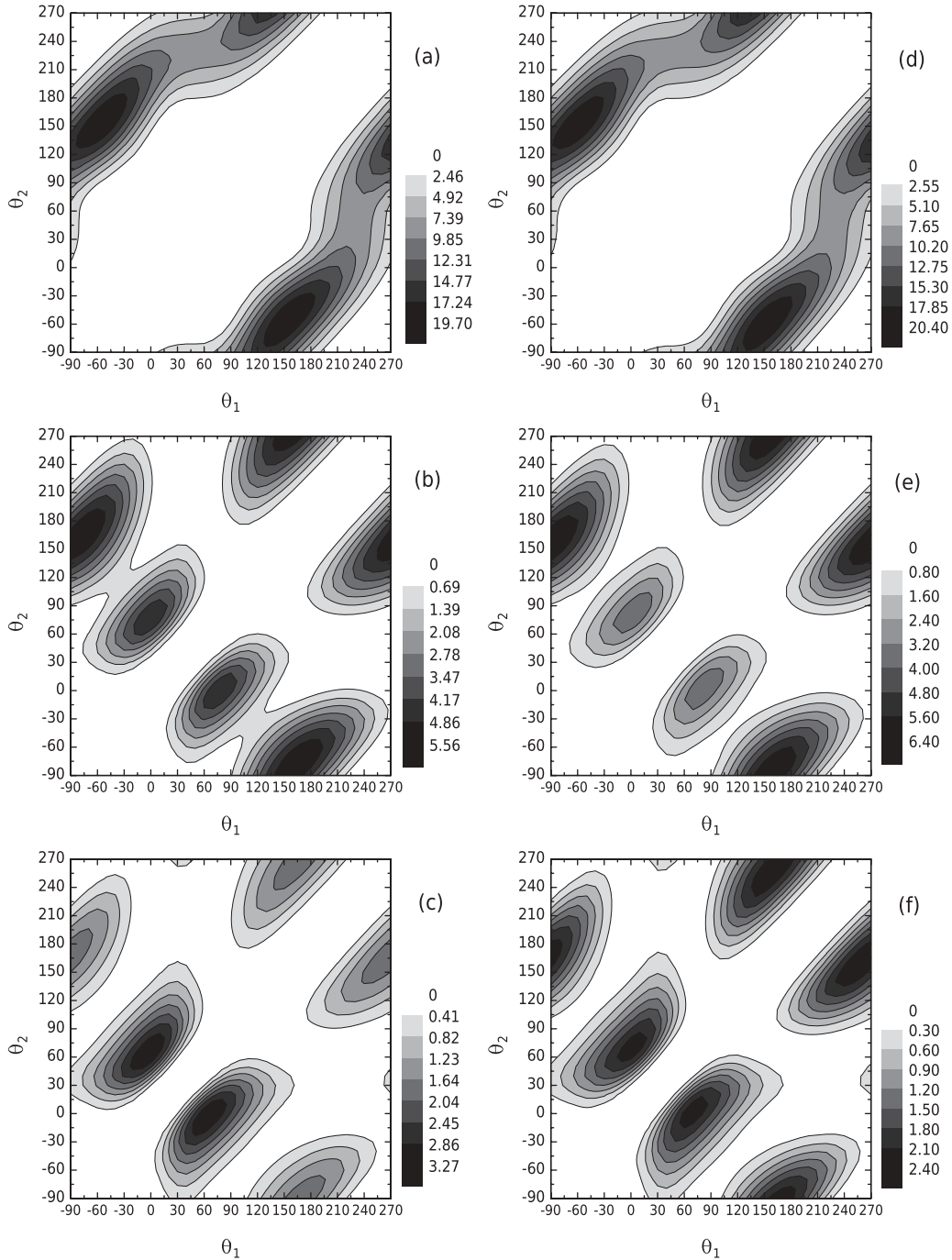


FIG. 2. Angular distributions of the two ejected electrons in the scattering plane. The polar angles are measured from the direction of the incident beam. The calculated ionization FDCS are given in units of 10^{-5} a.u. for proton and antiproton impinging on He at $E_i = 700$ keV. The momentum transfer Q is 0.9 a.u. The contour plots (a)–(c) correspond to proton impact and (d)–(f) to antiproton impact. The (a) and (d) plots correspond to ejected electrons with 3 eV in equal energy regime, (b) and (e) to 10 eV electron ejection energies, and (c) and (f) to the case of 15 eV electron energies.

The binary peak in the final momenta distribution can be explained in terms of the TS1 mechanism: the projectile hits an electron which then hits the other one and both emerge in almost perpendicular directions. The direction of the total electronic momentum $\mathbf{k}_1 + \mathbf{k}_2$ equals the projectile momentum transfer and the target core remains as a spectator in this case (the recoil momentum $\mathbf{p}_R \approx 0$). The recoil peak can be explained in a similar way: the projectile hits an

electron, which then hits the target core first ($\mathbf{p}_R \approx 2\mathbf{Q}$) and then removes the second electron ($\mathbf{k}_1 + \mathbf{k}_2 \approx -\mathbf{Q}$). As a result, for fixed \mathbf{Q} , the recoiling ion acquires higher momentum than in the former case. A third mechanism which has been denominated “back-to-back” has been proposed and consists in the removal of an electron by the projectile which then hits the target nucleus ($\mathbf{k}_1 \approx -\mathbf{Q}, \mathbf{p}_R \approx 2\mathbf{Q}$). In a subsequent stage, the recoiling nucleus hits the other electron and the final

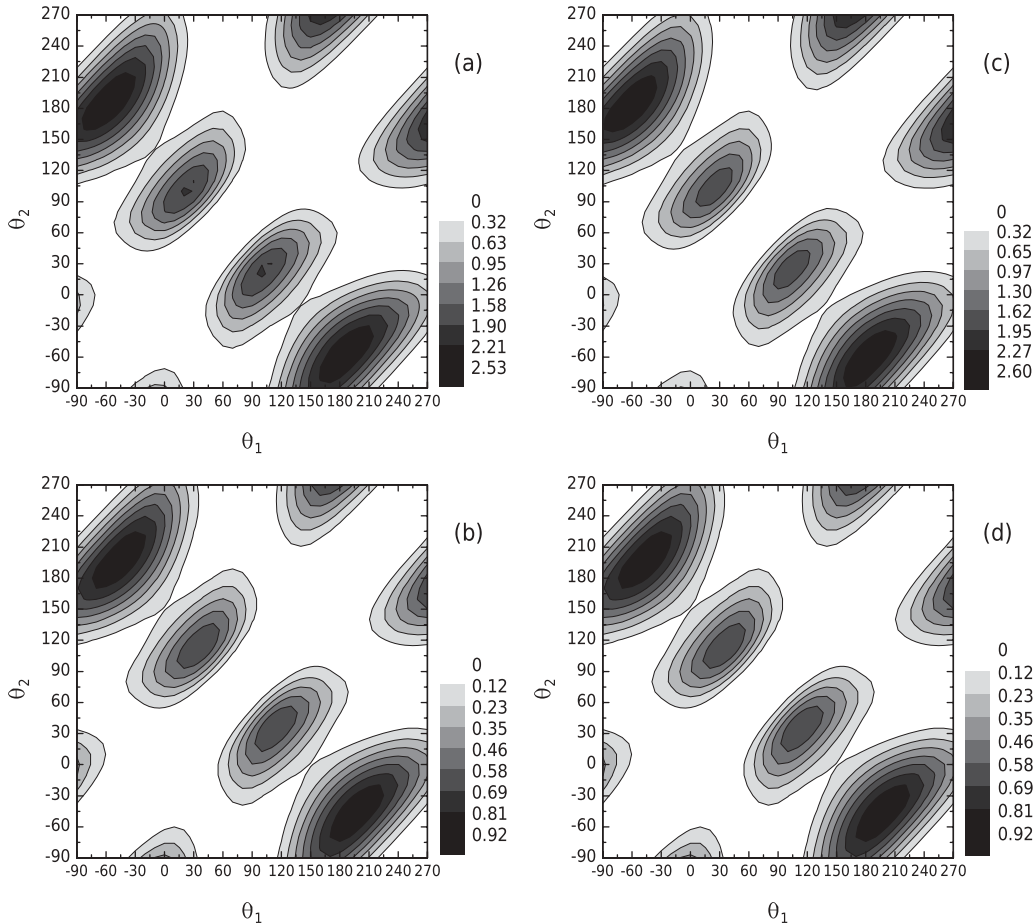


FIG. 3. Contour plots of the angular distributions of the two electrons for double ionization of He by proton impact (a), (b) and antiproton (c), (d) impact. The impact energies considered are $E_i = 2000$ keV (a) and (c), and $E_i = 6000$ keV (b) and (d). The emission geometry considered is that of Fig. 2. The FDCS are in units of 10^{-5} a.u.

configuration is given by $\mathbf{k}_1 + \mathbf{k}_2 \approx 0, \mathbf{p}_R \approx \mathbf{Q}$. This situation corresponds to both electrons leaving the atom in opposite directions with the recoil acquiring the projectile momentum transfer. This mechanism results from the threshold Wannier configuration and it is forbidden in atomic photo-double-ionization by a selection rule. For charged particle impact the selection rule disappears, and this structure turns important in some approximations that overestimate the interelectronic repulsion as the 3C model [33]. A quick inspection of Fig. 2 clearly evidences that the back-to-back mechanism is not present for the present model, and this is due to the coupling introduced via Eq. (36). For a more detailed scheme on these first-order collisions, we refer the reader to [40].

The binary peaks are then associated to electrons emerging preferentially close to the main diagonal region at which the double emission is forbidden by the interelectronic repulsion. The recoil peaks, on the other hand, are placed far from the diagonal and represent electrons being emitted in the backward direction. As an example, in Fig. 2(b) the binary peak is centered at $(\theta_1 \approx -5^\circ, \theta_2 \approx -75^\circ)$, while the recoil is located at $(\theta_1 \approx -70^\circ, \theta_2 \approx 165^\circ)$.

When the impinging projectiles are protons, the binary peak is enhanced with respect to the antiproton counterpart. The postcollisional interaction introduced by the effective-momentum theory in the final state tends to focus the electron

in the forward or backward direction depending on the projectile nature.

In contrast to the 10 eV and 15 eV cases, for 3 eV emitted electrons, the angular distributions show momenta in practically opposite directions and no binary structure is observed. Provided that the TS1 mechanism is mediating the double-electron emission, this result is consistent with the Wannier theory in which the electrons near the threshold region emerge in opposite directions. As the emission energy is increased, the electrons depart from the collinear geometry as expected.

In Fig. 3 we show similar distributions for increasing projectile energies. Both electrons are emitted with 10 eV, while the projectile energies considered are 2 MeV for the panels (a) and (b) and 6 MeV in (c) and (d) cases. As in Fig. 2, the first (second) column corresponds to proton (antiproton) impact. At these collision energies we observe that the structures move toward the \mathbf{Q} direction (parallel or antiparallel). Tiny differences are obtained between proton and antiproton impact at a collision energy of 2 MeV for this particular configuration. Differences are practically nonexistent at an impact energy of 6 MeV. This situation is in contrast with the experimental results of Fischer *et al.* [41], which suggest a possible dependence of the FDCS on the projectile charge sign at an impact energy of about 6 MeV.

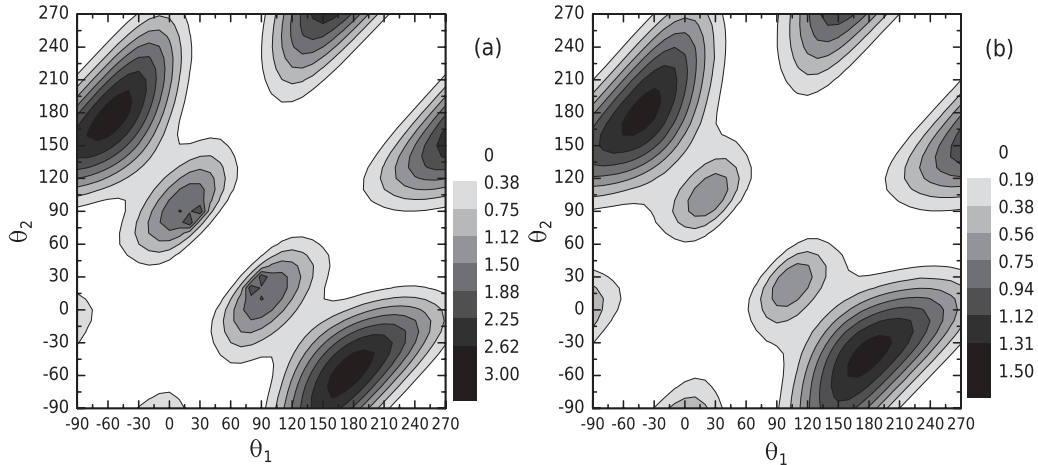


FIG. 4. Contour plots of the angular distributions of the two electrons for double ionization of He by proton impact at 700 keV/amu. The electrons are ejected with equal energies of 10 eV in the collision plane and the momentum transfer Q is (a) 1.2 a.u. and (b) 1.6 a.u. The FDCS are in units of 10^{-5} a.u.

In Fig. 4 we analyze the dependence of the FDCS with the momentum Q transferred by the projectile (proton impact only). We show the electron angular distribution for $Q = 1.2$ a.u. [Fig. 4(a)] and $Q = 1.6$ a.u. [Fig. 4(b)], when both electrons emerge with equal energies of 10 eV. These distributions can be compared to the distribution shown in Fig. 2(b). We note that as the Q value increases, the relative importance of the binary peak decreases compared with the recoil peak. We note that the electrons are not able by themselves to account for the whole momentum transfer and the recoiling target nucleus must participate in the collision. On the other hand, the Gramm-Schmidt orthogonalization process eliminates the contribution of direct collisions between the heavy particles and the only way for the recoiling nucleus to acquire momentum is via electron impact. As a result, the main mechanism that leads to double-electron emission for large Q and low emission energies is the recoil mechanism.

IV. REPRESENTATION TYPES IN DOUBLE IONIZATION

The development of the reaction microscope during the 1990s [42] allowed for a completely new insight of collision processes. In particular, atomic double-ionization processes by either ion or electron impact were experimentally explored [41, 43]. As a result, different graphical representations have been used in order to highlight the main physical trends exhibited by the data. In the following, we briefly analyze some of these representations.

For two emitted electrons the simplest representation is given by a two-dimensional Cartesian or polar graph, where either the angular or the energetic distribution is displayed for one of the emitted electrons keeping the emission energy and direction of the other electron fixed [44]. This angular representation is similar to that widely used in $(e, 2e)$ studies since the 1970s and is probably the easiest to assimilate. In fact, applied in recent years in $(e, 3-1e)$ studies, it helped to identify second-order contributions in the projectile-atom interactions [45].

When two variables are required in the analysis [either (θ_1, θ_2) [41,43] or (E_1, E_2) [46]], the usual graphical representation is the so-called contour plot, as used in the previous section. Nevertheless, we note that this representation does not provide a complete description of the process. In particular, the role played by the target ion recoil momentum during the collision process is hard to infer. To help identify the binary, recoil, and back-to-back mechanisms, in our former works [33,40] we have drawn contour lines for the FDCS over the recoil ion momentum magnitude contour plot in terms of (θ_1, θ_2) . This procedure allowed us to analyze the four-body dynamics in the angular distributions highlighting the analogies between $\mathbf{k}_1 + \mathbf{k}_2$ in the different regions and the single ionization counterpart for the FDCS. In Figs. 5(a) and 5(b) we show the FDCS corresponding to Figs. 2(b) and 2(e) as contour lines over the recoil distribution for proton and antiproton impact. We observe that the binary peak is located in the low recoil region, while the recoil peak remains near the region associated to large values of the recoil momentum. In both cases, a small displacement is observed relative to the extreme values. This shift can be ascribed to the postcollisional effect of momenta exchange provided by the model.

Another possible representation is provided by the denominated ternary plots where the distributions are displayed in a triangle, as used for tau meson decay [34]. In these plots each of the magnitudes is represented as the relative distance to a given triangle side. In recent years, this representation was applied to describe the FDCS for single atomic ionization of He by C^{6+} impact [35], and it is available in many scientific drawing programs.

We now represent the FDCS obtained in the preceding section with ternary plots, for which we use the variables Q , p_R , and $\mathbf{k}_1 + \mathbf{k}_2$:

$$\pi_{k_1+k_2} = \frac{|\mathbf{k}_1 + \mathbf{k}_2|^2}{P^2}, \quad \pi_Q = \frac{|Q|^2}{P^2}, \quad \pi_{p_R} = \frac{|p_R|^2}{P^2}, \quad (37)$$

where

$$P^2 = |Q|^2 + |p_R|^2 + |\mathbf{k}_1 + \mathbf{k}_2|^2. \quad (38)$$

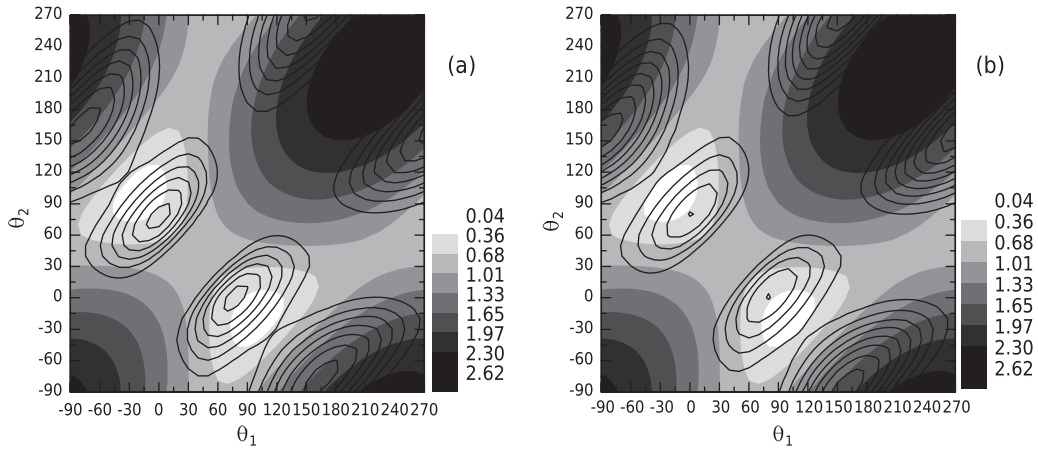


FIG. 5. Angular distributions of the FDCS for two electrons drawn over the corresponding absolute values of the target recoil momentum, for the same dynamical conditions and projectiles considered in Figs. 2(b) and 2(e). The scale on each plot indicates the absolute values for the target recoil momentum.

According to Viviani's theorem the sum of these variables is the height of the triangle, which is assumed to be one. Another normalization criteria could be used [47].

The momentum-conservation law $\mathbf{Q} = \mathbf{p}_R + \mathbf{k}_1 + \mathbf{k}_2$ restricts inside of a circle the scatter dots that represent the FDCS in the ternary plot.

From the momentum-conservation law the first-order transitions due to the projectile can be related to recoil momentum values close to 0, Q , or $2Q$, when the momentum of each electron is close in magnitude to Q . In the present representation, the binary peak is expected to be close to the π_{p_R} axis. On the other hand, the recoil peak corresponds to $\pi_{k_1+k_2} = \pi_Q$ and π_{p_R} takes its largest possible value. Finally, the back-to-back emission is associated to the smallest values of $\pi_{k_1+k_2}$. We note that in this representation the presence of events displaced from the regions above mentioned indicates that higher collision orders are present. In contrast to what happens in photo-double-ionization processes, we note that for charged particle impact the back-to-back emission for equal energy electrons is not forbidden by any selection rule. However, as stated above, models which overestimate

the interelectronic repulsion tend to increase the relative contribution of this mechanism to the FDCS.

In Figs. 6(a) and 6(b) we show the ternary plot for the FDCS evaluated with the present model for the double ionization of He by 700 keV H^+ projectiles. The electron emission energies are $E_1 = E_2 = 10$ eV and the momentum transfer $Q = 0.9$ a.u. We point out the presence of a cutoff for π_Q which is clearly related to the fixed Q value chosen. Furthermore, the condition $|\mathbf{k}_1 + \mathbf{k}_2| \leq k_1 + k_2$ trims a sector of the circular allowed region. For the present case, we can easily translate into this representation the main features observed in Fig. 5. For both projectiles the main emission is observed in the region associated to large recoil values. We note, however, that for proton impact the binary peak is much more intense than for antiproton impact. In addition, and as stated above, the binary structure is not located in the punctual zero recoil ion momentum region as a consequence of the momentum exchange between the four particles. Antiprotons enhance the recoil peak as a consequence of the projectile-electron repulsion: during the collision the electron is pushed against the He nucleus. Proton projectiles, on the other hand, pull the

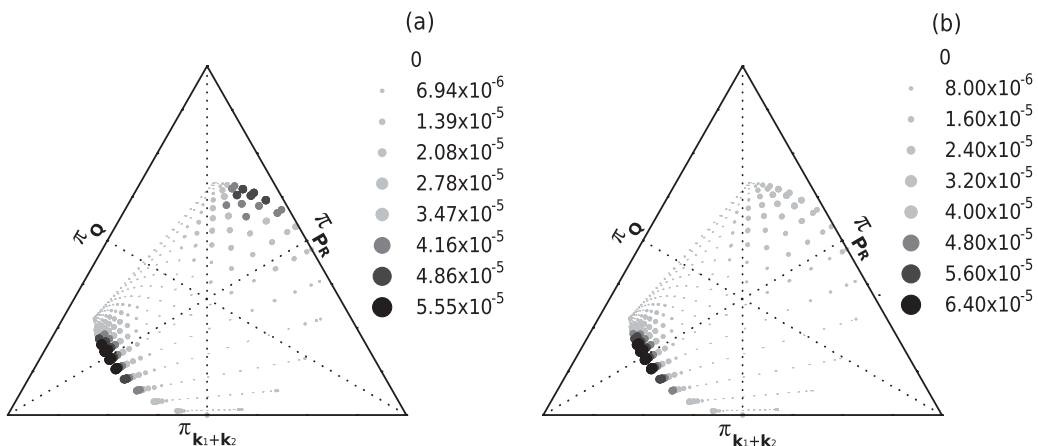


FIG. 6. Ternary plots for the distributions corresponding to Figs. 2(b) and 2(e). The left panel corresponds to proton impact and the right one to antiproton, respectively. The FDCS are expressed in atomic units.

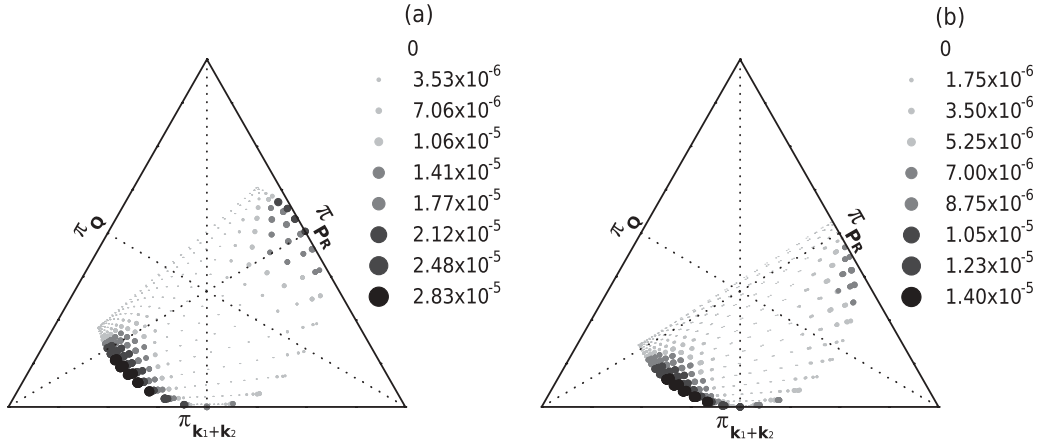


FIG. 7. Ternary plots for the distributions corresponding to Figs. 4(a) and 4(b), respectively. FDCS are expressed in atomic units.

electrons outwards of the parent ion leading to a comparatively more relevant electron-projectile interaction.

In Figs. 7(a) and 7(b) we show the ternary plot for the FDCS corresponding to the cases shown in Figs. 4(a) and 4(b), respectively. We note that the above discussed mechanisms are easily recognized, and we observe from the comparison of these figures with Fig. 6(a) that as Q increases the allowed region is reduced and the constraints imposed by Eq. (38) and by the maximum total electronic momentum are clearly visible. The binary structure diminishes and the double emission is mediated by the recoiling target core as discussed in the previous section. In this sense, the present ternary representation complements the interpretation of the contour plots previously shown by evidencing the role of the recoiling target nucleus in the double-electron emission. Nevertheless, we notice that other possible combinations of variables, or particular projections of the involved momenta, can be also used to generate alternative ternary representations.

Finally, we point out that, for the $H^+ + He \rightarrow H^+ + He^{2+} + 2e$ process, Schulz and collaborators recently proposed a quaternary representation of the DDCS in terms of a three-dimensional (3D) plot [31,48]. This representation is particularly convenient when diverse mechanisms as TS1, shake off (SO), and two-step-2 (TS2) participate in the description of the double-ionization process. The 3D representation helps to identify and separate the relative contribution of mechanisms involving first-order (TS1 and SO) and higher-order (TS2) collisions. We have explored the quaternary representation (not shown here) for the cases shown in the previous section, without any visible advantage over the 2D representation here proposed. It could be useful though to tackle emission geometries for which the TS1, SO, and TS2 become competitive.

V. CONCLUSIONS

We have studied the Schrödinger equation for a four-body system interacting via Coulomb potentials. Separable solutions which can be expressed as a product of six independent functions have been proposed. These solutions satisfy an equation with a separable operator plus a coupled nondiagonal term. We have shown that when some of the relative two-body

motions are modeled by Coulomb waves the remaining independent functions must account for the nonorthogonal kinetic energy and satisfy coupled differential equations. Different asymptotic limits have been explored in order to include as much information as possible of the nondiagonal operator which is neglected in the 6C model. The resulting equations have been analyzed for different physically meaningful asymptotic conditions in the problem. For some of these regions, we have developed approximated wave functions that account for the nondiagonal kinetic energy in terms of Coulomb-like distortion factors with effective momenta. These models are based on considering fixed values for the coupling variables in the respective equations. We have considered this as the most physically sound choice, even when many other alternatives are possible to approximately decouple the equations, as indicated in the text.

The present model has been used to evaluate the FDCS for the double ionization of He by ion impact, focusing on the possible differences arising from the projectile charge sign at different impact energies. The results are represented as contour plots in the electrons emission angles, which shows the characteristic dynamic of a four-body reaction. The present results clearly exhibit the denominated binary and recoil structures, but show no evidence of a back-to-back emission mechanism. This is a consequence of the electron-electron interaction being weakened by the coupling terms hereby considered. We observe that the FDCS for proton impact are quite different from those corresponding to antiproton impact, as corresponds to a four-body formalism at the lowest impact energies considered. As the impact energy increases the projectile charge sign turns less relevant as expected.

We discussed the different representation schemes which have been used during the past decade to highlight the physics underlying the double-ionization processes at the fully differential level. In particular, we suggest a 2D ternary plot representation as a complementary tool to simultaneously identify the role played by the recoil ion, the projectile, and the emitted electrons during the double-ionization process. Such a detailed insight on the four-body dynamics is hardly possible using the standard contour plot representation so far used in the field.

Finally, we note that despite the long times needed to acquire statistics, more fully differential experimental data is urgently needed to further refine the distorted-wave models currently under use. In this sense, we point out that during the past decade most of the theoretical work cited as well as the different representations explored have been based upon a single set of measurements [41]. A wider data set would be

welcome and would surely improve our understanding of the present collision system.

ACKNOWLEDGMENTS

This work has been supported by PIP 112-200801-02760 of CONICET and PGI 24/F049 of UNS (Argentina).

-
- [1] L. Vainshtein, L. Presnyakov, and I. Sobelman, *Zh. Eksper. Teor. Fiz.* **45**, 2015 (1963) [*Sov. Phys. JETP* **18**, 1383 (1964)].
- [2] M. M. Felden and M. A. Felden, *Phys. Rev. A* **4**, 1476 (1971).
- [3] M. M. Felden, M. A. Felden, and J. C. Braun, *Physica* **61**, 355 (1972).
- [4] M. Felden, *Phys. Lett. A* **51**, 226 (1975).
- [5] C. R. Garibotti and J. E. Miraglia, *Phys. Rev. A* **21**, 572 (1980).
- [6] Dz. Belkić, *J. Phys. B: At. Mol. Phys.* **11**, 3529 (1978).
- [7] M. Brauner, J. S. Briggs, and H. Klar, *J. Phys. B: At. Mol. Opt. Phys.* **22**, 2265 (1989).
- [8] M. Brauner, J. S. Briggs, and H. Klar, *Z. Phys. D* **11**, 257 (1989).
- [9] L. Rosenberg, *Phys. Rev. D* **8**, 1833 (1973).
- [10] D. S. F. Crothers and J. F. McCann, *J. Phys. B: At. Mol. Phys.* **16**, 3229 (1983).
- [11] P. D. Fainstein, V. H. Ponce, and R. D. Rivarola, *J. Phys. B: At. Mol. Opt. Phys.* **21**, 287 (1988).
- [12] E. O. Alt and A. M. Mukhamedzhanov, *Phys. Rev. A* **47**, 2004 (1993).
- [13] J. Berakdar, *Phys. Rev. A* **53**, 2314 (1996).
- [14] A. Engels, H. Klar, and A. W. Malcherek, *J. Phys. B* **30**, L811 (1997).
- [15] P. A. Macri, J. E. Miraglia, C. R. Garibotti, F. D. Colavecchia, and G. Gasaneo, *Phys. Rev. A* **55**, 3518 (1997).
- [16] J. Berakdar and J. S. Briggs, *Phys. Rev. Lett.* **72**, 3799 (1994).
- [17] S. Jones, D. H. Madison, and D. A. Konovalov, *Phys. Rev. A* **55**, 444 (1997).
- [18] S. P. Lucey, J. Rasch, C. T. Whelan, and H. R. J. Walters, *J. Phys. B: At. Mol. Opt. Phys.* **31**, 1237 (1998).
- [19] G. Gasaneo, F. D. Colavecchia, C. R. Garibotti, J. E. Miraglia, and P. Macri, *Phys. Rev. A* **55**, 2809 (1997).
- [20] J. E. Miraglia, M. G. Bustamante, and P. A. Macri, *Phys. Rev. A* **60**, 4532 (1999).
- [21] Dz. Belkić, I. Mancev and V. Mergel, *Phys. Rev. A* **55**, 378 (1997).
- [22] A. Martinez, R. Rivarola, R. Gayet, and J. Hanssen, *Phys. Scr. T* **80**, 124 (1999).
- [23] Dz. Belkić, I. Mancev and J. Hanssen, *Rev. Mod. Phys.* **80**, 249 (2008).
- [24] J. Berakdar, *Phys. Lett. A* **220**, 237 (1996).
- [25] J. R. Götz, M. Walter, and J. S. Briggs, *J. Phys. B* **39**, 4365 (2006).
- [26] J. F. Reading and A. L. Ford, *Phys. Rev. Lett.* **58**, 543 (1987).
- [27] C. Díaz, F. Martín, and A. Salin, *J. Phys. B* **35**, 2555 (2002).
- [28] M. S. Pindzola, F. Robicheaux, and J. Colgan, *J. Phys. B* **40**, 1695 (2007).
- [29] M. Foster, J. Colgan, and M. S. Pindzola, *J. Phys. B* **41**, 111002 (2008).
- [30] X. Guan and K. Bartschat, *Phys. Rev. Lett.* **103**, 213201 (2009).
- [31] M. F. Ciappina, T. Kirchner, and M. Schulz, *Phys. Rev. A* **84**, 034701 (2011).
- [32] L. Gulyás, A. Igarashi, and T. Kirchner, *Phys. Rev. A* **86**, 024701 (2012).
- [33] S. D. López, C. R. Garibotti, and S. Otranto, *Phys. Rev. A* **83**, 062702 (2011).
- [34] R. H. Dalitz, *Philos. Mag.* **44**, 1068 (1953).
- [35] S. Otranto, R. E. Olson, and J. Fiol, *J. Phys. B: At. Mol. Opt. Phys.* **39**, L175 (2006).
- [36] L. U. Ancarani and G. Gasaneo, *J. Phys. A: Math. Theor.* **43**, 085210 (2010).
- [37] M. R. H. Rudge and M. J. Seaton, *Proc. R. Soc. A* **283**, 262 (1965).
- [38] A. R. P. Rau, *Phys. Rev. A* **4**, 207 (1971).
- [39] S. Otranto, G. Gasaneo, and C. R. Garibotti, *Nucl. Instrum. Methods, Phys. Res. B* **217**, 12 (2004).
- [40] S. D. López, C. R. Garibotti, and S. Otranto, *Nucl. Instrum. Methods, Phys. Res. B* **283**, 63 (2012).
- [41] D. Fischer *et al.*, *Phys. Rev. Lett.* **90**, 243201 (2003).
- [42] R. Moshhammer, M. Unverzagt, W. Schmitt, J. Ullrich, and H. Schmidt-Böcking, *Nucl. Instrum. Methods, Phys. Res. B* **108**, 425 (1996).
- [43] A. Dorn, A. Kheifets, C. D. Schröter, B. Najjari, C. Höhr, R. Moshhammer, and J. Ullrich, *Phys. Rev. Lett.* **86**, 3755 (2001).
- [44] A. Lahmam-Bennani, C. Dupre, and A. Duguet, *Phys. Rev. Lett.* **63**, 1582 (1989).
- [45] A. Lahmam-Bennani, E. M. Staicu-Casagrande, A. Naja, C. Dal Capello, and P. Bolognesi, *J. Phys. B: At. Mol. Opt. Phys.* **43**, 105201 (2010).
- [46] L. Sarkadi and A. Orbán, *Phys. Rev. Lett.* **100**, 133201 (2008).
- [47] E. W. Weisstein, *Viviani's Theorem*, from MathWorld—A Wolfram Web Resource <http://mathworld.wolfram.com/VivianisTheorem.html>
- [48] M. Schulz, D. Fischer, T. Ferger, R. Moshhammer, and J. Ullrich, *J. Phys. B: At. Mol. Opt. Phys.* **40**, 3091 (2007).